(NASA-CR-163711) EXPERIMENTS ON INITIAL AND BOUNDARY CONDITIONS (Polytechnic Inst. of New York.) 11 p HC A02/MF A01

N81-11341

Unclas
G3/34 38324

MASTER

80·38

NSG-1248

Gino Moretti
Polytechnic Institute of New York

Abstract

Effects of three different models for the treatment of subsonic boundary conditions, applied to the problem of flow in a channel with a bump, are discussed. A preliminary discussion of the numerical treatment of the corners is presented.

1. Introduction

Experimentalists have learnt to appreciate the importance of a proper installation, a careful calibration of instruments and an analysis of environmental interferences. Data obtained by the Wright Brothers on their historical wind tunnel enabled them to evaluate the possibility of flying; by current standards they would probably not even fit in what engineers mention as "ballpark" range. The designer's problem is efficiency; errors larger than 1% in basic information should not be tolerated.

Surprisingly, a large amount of numerical work is far from reaching such standards. More surprisingly, very little seems to be done to improve the situation, and this is so much more disturbing since some claims are occasionally made that numerical analysis should replace experiments.

The present paper is a modest attempt to show a possible approach to understand reliability of numerical analysis. It is shaped as a series of numerical experiments. Empiricism, however, is not suggested. Empiricism is manifested by juggling of arbitrary coefficients, mesh refinements and, manipulation of arbitrary additional terms. The work described in this paper, instead, is inspired by the idea that a numerical procedure describes, more or less accurately, a physical model and that the understanding of such a model will lead us to judge whether or not our calculation makes the physical sense which it should. To go back to our former comparison with experiments, a typical wind tunnel correction inspired by the same criterion to which the present study is inspired is the wall correction for viscous and transonic effects.

In preparing the present paper, a very large amount of cases were computed, expressing different lines of thought and, for each one of them, tests of different parameters. A detailed discussion transcends the limits of a presentation. Therefore, I will limit myself to showing the guidelines of the investigation, and some of its highlights, without attempting to be exhaustive and even to draw conclusions which, as it will appear from the context, could, at this stage, still be hasty and inappropriate.

2. A channel flow

On September 18-19, 1979, a Workshop was held in Stockholm, the object of which was the comparison of results obtained by using different numerical methods on two assigned problems, the second of which was formulated as follows.

"Internal two-dimensional flow through a parallel channel having a 4.2% thick circular arc 'bump' on the lower wall. The ratio of static downstream pressure to total upstream pressure is 0.623512 (corresponding to M=0.85 in isentropic flow), and the distance between the walls is 2.073 times the chord length of the bump."

Obviously, the emphasis of the assignment was on steady solutions and transonic flow with an imbedded shock. The latter requirement adds a number of complications to the problem of a subsonic, steady, isentropic flow in a channel. The assigned data were so close to producing a choked flow that some of the methods generated a choked flow (all potential fully conservative methods) and others did not (all potential nonconservative methods and Euler solvers, and Hafez's artificial compressibility method). Scattering of results and conflicts between conclusions are not new in our short history of numerical analysis. As I recall, the first numerical contest was inspired by Morton Cooper in 1965, a calculation of blunt body shock layers for an ellipsoid of revolution with a 2:1 axis ratio, at a free stream Mach number of 3 [1]. Techniques ranging from truncated series expansions to integral relations to inverse methods offered a variety of results. Comparing them with what has now been accepted as standard, that is, a second-order finite difference calculation with bow-shock fitting, we see that methods focussed on the stagnation line gave good results near the stagnation line and poor results away from it, whereas methods focussed on the sonic line had the opposite behavior [2]. The contest clearly showed a need for a different numerical approach, more general and powerful.

The object of a Workshop is, indeed, to

promote healthy competition and unrestrained debates; not to solve problems or to emit verdicts; a Workshop can be considered successful if it inspires new, and deeper, work. In studying the results of the Stockholm workshop, I decided to take a closer look at the channel flow, at least limitedly to a certain brand of Euler solvers.

Obvious questions to be answered were:

1) Is a steady state reached?

2) Do results depend on the type and size of the computational mesh?

3) How do different treatments of the left and right boundary of the computed region affect the results?

4) Can any detail be provided of the flow near the leading and trailing edges of the bump?

Note that I abstain from mentioning integration schemes. Relative virtues and shortcomings of such schemes, including their ability to capture shocks, their numerical diffusion and dispersion, etc. are out of context. They cannot be tested in the channel flow problem unless the questions above have been exhaustively answered. On the other hand, there are general features of the flow which should be revealed and which should provide clues to the questions, regardless of the integration scheme having been used, at least so long as the flow is far from transonic.

I decided, thus, to limit a preliminary investigation to subsonic, isentropic flows, and I adopted the MacCormack, predictor-corrector scheme to the equations of motion in the form:

$$P_t + \vec{V}.\nabla P + \gamma \nabla.\vec{V} = 0 \qquad (1)$$

$$\vec{V}_t + (\vec{V}.\nabla)\vec{V} + T \nabla P = 0$$

where P is the logarithm of the pressure, $\vec{V}$ the velocity, T the temperature and γ the ratio of specific heats. Pressure and temperature are related by

$$P = \frac{\gamma}{\gamma-1} \ln T \qquad (2)$$

For subsonic flows, the MacCormack scheme is safely applicable to (1) and has the advantage of great simplicity. To maintain second-order accuracy at the boundaries, where the MacCormack scheme can be applied only at the predictor (or corrector) level, for want of external data in the other level, any derivative at such a level is discretized by differences of the type:

$$2 f_1 - 3 f_2 + f_3$$

where values at three adjacent points, from the boundary in, are denoted by 1,2 and 3, sequentially.

3. Computational grid

The grid suggested for the Stockholm workshop was a Cartesian grid, normalized between upper and lower wall of the channel, and stretched from $-\infty$ to $+\infty$ with an strong accumulation of grid lines over the bump. I used this type of grid, forcing two grid lines to originate exactly at the

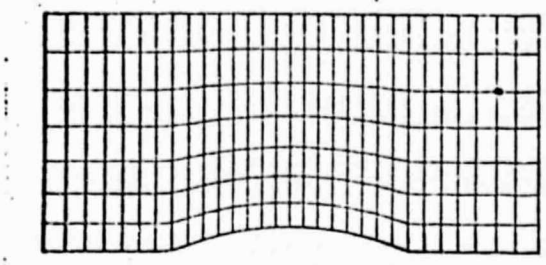

Fig. 1

leading and trailing edges (Fig. 1).

I also adopted a different grid (shown in Fig. 2) which is obtained using a conformal mapping of the Kármán-Trefftz type:

$$\frac{z-1}{z+1} = \left(\frac{\zeta-1}{\zeta+1}\right)^{\delta} \qquad (3)$$

where $z=x+iy$ is the complex coordinate in the physical plane, $\zeta=\xi+i\eta$ is the complex coordinate in the mapped plane, and δ is related to the thickness-to-chord ratio of the bump, τ, by:

$$\delta = \frac{1}{2} + \frac{1}{\pi} \arctan \frac{1-4\tau^2}{4\tau} \qquad (4)$$

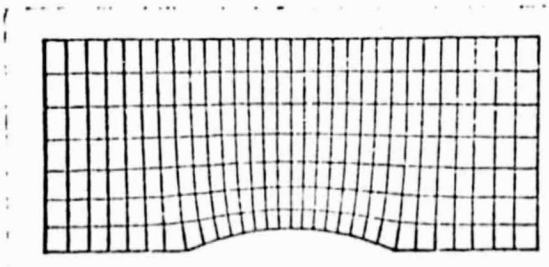

Fig. 2

The η-coordinates are normalized between the upper and lower walls, and the ξ-coordinates are stretched in the horizontal direction as in the Cartesian grid. Calling u and v the velocity components in the direction of the Cartesian axes for

the first grid, and in the direction of the ξ = constant, η = constant axes for the second grid, it turns out that v vanishes exactly along the upper wall when the first grid is used, and along the lower wall, when the second grid is used. Consequently, one may expect the calculation to be easier and, perhaps, the results to be better along the wall where v vanishes. In any event, the boundary conditions at rigid walls are enforced by first integrating the Euler equations as at interior points, and then by correcting the pressure to satisfy the vanishing of the velocity component normal to the wall [3,4]. Along walls where v is not identically zero, the u-momentum equation is replaced by an equation along the tangent to the wall.

Calculations are actually performed in a computational plane, (X, Y), where the grid is evenly spaced in both directions. If the first grid is used, additional coefficients appear, containing dX/dx, $\partial Y/\partial x$ and $\partial Y/\partial y$. If the second grid is used, two independent sets of additional coefficients and terms appear, the first due to normalization and stretching, and containing $dX/d\xi$, $\partial Y/\partial\xi$, $\partial Y/\partial\eta$, the second due to the mapping, and containing

$$g = G e^{i\omega} = \frac{d\zeta}{dz} , \quad \phi = \phi_1 + i \phi_2 = \frac{d \log g}{d\zeta} \qquad (5)$$

The major physical difficulty is offered by the leading and trailing edge corners, where the flow stagnates. In using the first grid, the difficulty is reflected in the discontinuity in the slope of the lower wall (which affects all points on the vertical grid lines issuing from the corners). If the second grid is used, a mapping singularity appears at the corners and the equations of motion, expressed in terms of ξ and η, become indeterminate. In both cases, thus, some special treatment must be given to the corner points and their immediate neighbors. If the grids are laid to avoid passing through the corners, the effect of neglecting them has to be evaluated.

4. Inlet and outlet boundary conditions

Another critical issue regards the treatment of the arbitrary computational boundaries which delimit an inlet and an outlet to the region of interest. Such boundaries cross regions of subsonic flow and some physical model is required to supply the information from outside which is necessary. New interest seems to have arisen on this problem in recent times, but the physical implications of modeling a subsonic boundary seem not to have been grasped firmly yet. The problem of subsonic boundaries cannot be disassociated from the problem of choosing initial conditions [5]. In internal flows, several simple physical models can be adopted, of which here is a sample:

1) The region of interest is a channel of a finite length, connecting two infinite cavities; the gas is at rest everywhere; at t=0, the stagnation pressure is increased in the cavity at left, until a given value is reached, and then kept constant,

2) The same setting is used, but at t=0 the pressure in the cavity at right is decreased until a given value is reached, and then kept constant,

3) The channel is infinitely long and it contains a gas at rest; at t=0, the channel is accelerated towards the left, until a cruising speed is reached.

In the first two cases, two models of transitions from the interior to infinite cavities are adopted at each boundary point on the left and on the right. As explained in [5], one can stipulate that the fictitious flows in the transitions are quasi-steady (the length of the transition being assumed as vanishingly small), so that, for the purpose of closing the boundary data sets, steady equations of motion can be differentiated in time. On the left, the total pressure and the slope of the velocity vector at each entry point are assigned. The latter condition brings in the largest arbitrariness in the model. Physically, one can always justify a choice of slopes by assuming that the inlet is equipped with a series of guiding vanes. In the present case, for example, one can assume that all velocity vectors are parallel to the rigid walls; this is obviously not the case for an infinitely long channel, and the effect of such a restrictive assumption on the rest of the flow has to be evaluated.

The equations used at the inlet are:

1) the definition of total pressure, differentiated in time under the assumption that the total pressure itself may be a function of time:

$$T P_t + u (1 + \sigma^2) u_t = T_o P_{ot} \qquad (6)$$

where the index o denotes stagnation values in the infinite capacity, and $\sigma = v/u$ is a prescribed value,

2) a left-running characteristic equation:

$$a P_t - \gamma u_t = R \qquad (7)$$

where R is the left-hand side of (7) as computed by the standard integration routine.

The outlet model is simpler, since the v-component of the velocity is determined on the basis of internal information only [6]; in the

present case, it is sufficient to prescribe the exit pressure as the pressure in infinite capacity, and compute the u-component of the velocity accordingly. The equations are, thus:

1) the continutity equation:

$$\rho u P_t + \gamma\rho u_t = \rho_- u_- P_{-t} + \gamma\rho_- u_{-t} \qquad (8)$$

2) the definition of total pressure:

$$T P_t + u u_t + v v_t = T_- P_{-t} + u_-(1 + \sigma_-^2) u_{-t} \qquad (9)$$

3) a right-running characteristic equation:

$$a P_t + \gamma u_t = R \qquad (10)$$

where R has the same meaning as in (7). In (8), (9) and (10), v_t is computed by the standard routine; u_{-t} is unknown but it can be eliminated easily. Naturally, here too there is an element of arbitrariness, whose effects have to be checked. For example, in an infinitely long channel, the pressure across the channel is not exactly constant at a finite distance from the bump.

The inlet and outlet boundaries just described allow perturbations proceeding from the interior to interact with the conditions in the infinite cavities. For each perturbation reaching the boundary, a new perturbation is generated and transmitted in the opposite direction. The process will eventually reach an asymptotic steady state, but the number of waves of a sizeable amplitude moving back and forth can be very large.

The third model relies on a simple idea: if the motion were one-dimensional, all perturbations would travel outwards as simple waves, at the end of the acceleration phase. A simple wave is easy to describe using information from the interior and the constancy of one Riemann invariant from the exterior. In a two-dimensional problem of internal flow, the waves cannot be exactly simple waves, but no major errors are expected if the velocity vector is forced to be parallel to the rigid walls at the inlet. The simple wave equations at the inlet are modified as follows:

$$a P_t - \gamma (1 + \sigma^2)^{1/2} u_t = R$$

$$a P_t + \gamma (1 + \sigma^2)^{1/2} u_t = 0 \qquad (11)$$

Similarly, at the outlet:

$$a P_t + \gamma u u_t/q = R$$

$$a P_t - \gamma u u_t/q = \gamma v v_t/q \qquad (12)$$

where v_t is computed by standard routines and q is the modulus of the velocity.

5. Two-dimensional calculations with models 1 and 2

We describe now the general features of calculations made using the first two models mentioned in Section 4. One of the problems presented by a study like the present one is the large amount of data produced by a single run and the necessity for organizing them in a series of simple plots, easy to interpret. I decided to store the following information:

1) at every step, P and u on the lower wall, at the inlet, at two selected points, and at the highest point on the bump,

2) at every step, location of selected isobars on the lower wall (to build an isobar pattern on an (x,t)-plane), and

3) at selected steps, P, u and v at all the grid points; this information can be easily processed to provide Mach numbers and total pressures.

The basic geometry has been defined as a channel with a width equal to 2, containing a bump which extends from x=-1 to x=1 and which has a maximum thickness of 0.2. This defines a corner angle of 157.38°, and δ=0.8743. To avoid initial complications at the corners, so that our attention can be focussed on the wave propagation and the effects of boundaries, we use a smooth lower wall which can be easily obtained from the mapping function by defining the wall as the image, in the z-plane, of a line η = b, where b is a constant greater than 0. The same definition can be transferred to the code which uses the Cartesian grid. In Fig. 3 there are some shapes of the lower wall for different values of b; one can observe that, for b less than 0.01, there is no practical difference between the wall

Fig. 3

so defined and the wall corresponding to b=0.

We begin with a very smooth wall, defined by b=0.1. The computational mesh has 7 intervals between the rigid walls and 30 intervals in the x-direction, stretched between x=-2.345 and x=2.345; 16 intervals cover the bump region. The stagnation pressure is raised (in the first method) or the exit pressure is lowered (in the second method) to produce final values of the Mach number "at infinity" of the order of 0.1. A plot of P vs. time at the 6th node on the lower wall is shown in Fig. 4, for the case where the first mehod is applied. The oscillations are obviously produced by waves going back and forth along the channel (at such low Mach numbers, the speed of propagation is practically the same in both directions, and the phenomenon shows a well defined frequency); one disturbing feature of the model is the smallness of the damping factor.

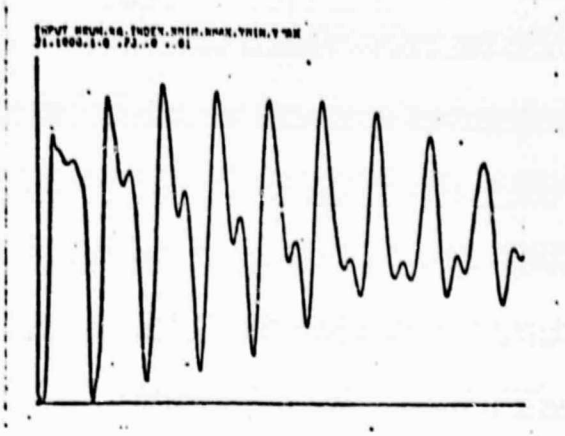

Fig. 4

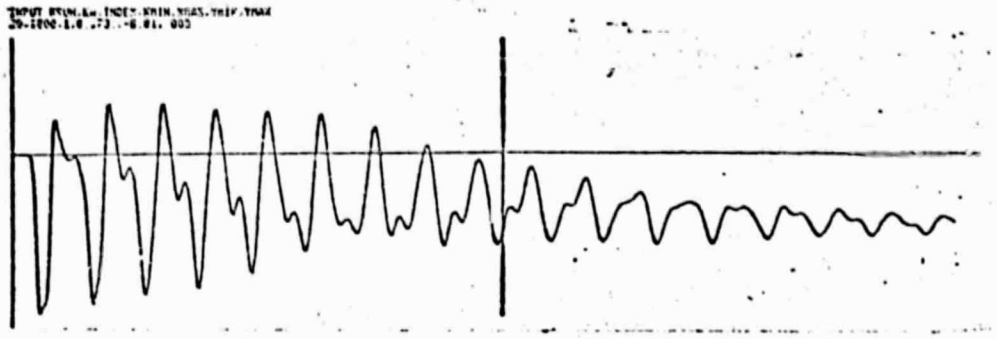

Fig. 5

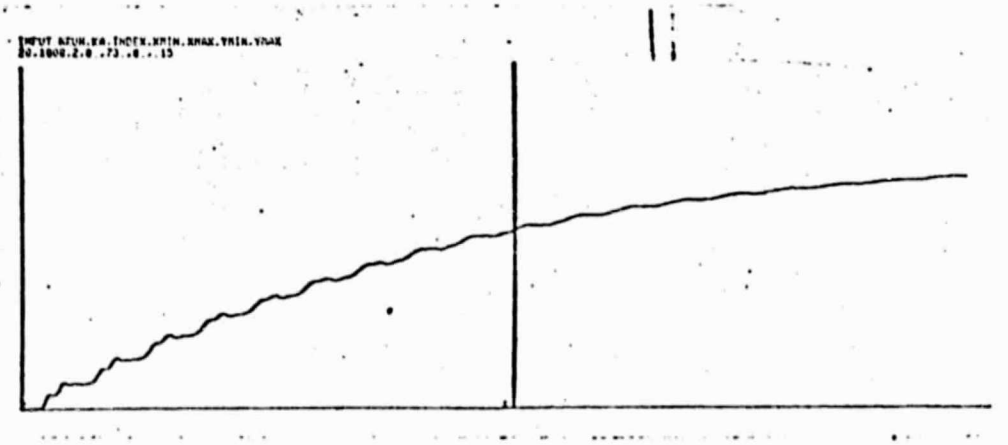

Fig. 6

A similar pattern appears (Fig. 5) using the second model; the oscillations are smaller in amplitude but still damped very slowly; Fig. 6 shows u(t) at the same node and from it we see that the velocity presents smaller oscillations but that a steady state is far from having been reached after 2000 computational steps (t=146).

Such details are hard to detect from plots of level lines at a given step. For example, isobars and isomachs at step 1000 (Figs. 7 and 8) look very reasonable, although the isobars would not pass a closer scrutiny, due to a clear lack of symmetry. As a matter of fact, if we plot P at the 6th node vs. P at the 24th node as they evolve in time, we see that, after 2000 steps, the plotting line still oscillates between -0.00283 and -0.00353, whereas at both points P should be about

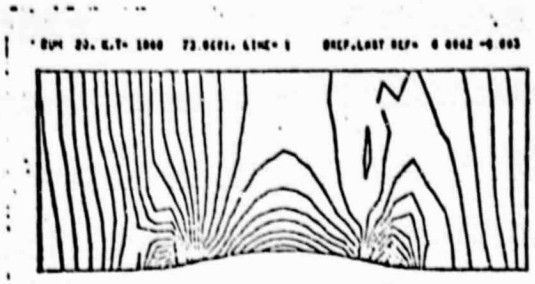

Fig. 7

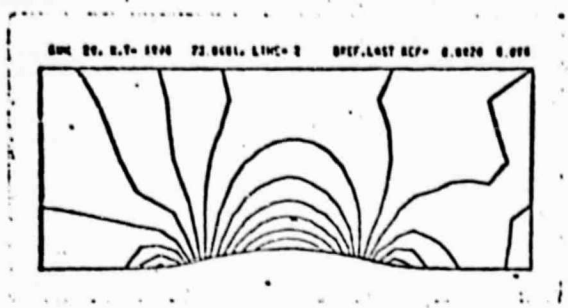

Fig. 8

-0.0032.

An analysis of these oscillations should take at least two elements into consideration: the first is the Mach number effect, and the second is the influence of geometry. To have an idea of the Mach number effect, let us rerun the above cases for a Mach number of 0.5. Plots of P and u vs. time are shown in Figs. 9 and 10 for the first model; Fig. 9 should be compared with Fig. 4. Oscillations still appear but they seem to be damped much more quickly. A similar behavior is seen in Figs. 11 and 12, which refer to the second model. One should, however, take care not to draw hasty conclusions from Figs. 4 and 9, or Figs. 5 and 11. The scale of P in Fig. 9 is 20 times smaller than in Fig. 4, and in Fig. 11 is 40 times smaller than in Fig. 5; the correct conclusion is that very small pressure waves take a long time to be eliminated. The patterns of level lines (isobars in Fig. 13, isomachs in Fig. 14) are much better than their counterparts for M=0.1 (Figs. 7 and 8). Even the v=constant lines, which are very critical, look good (Fig. 15). At this stage, it pays to take a look at lines of constant stagnation pressure (Fig. 16); here a new element appears. In fact, the stagnation pressure is practically constant everywhere, but it drifts away in the vicinity of the "corners" (or whatever remains of them in the smoothed wall). The stagnation pressure is a very

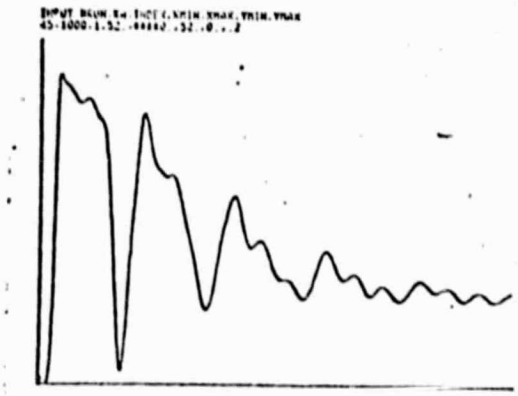

Fig. 9

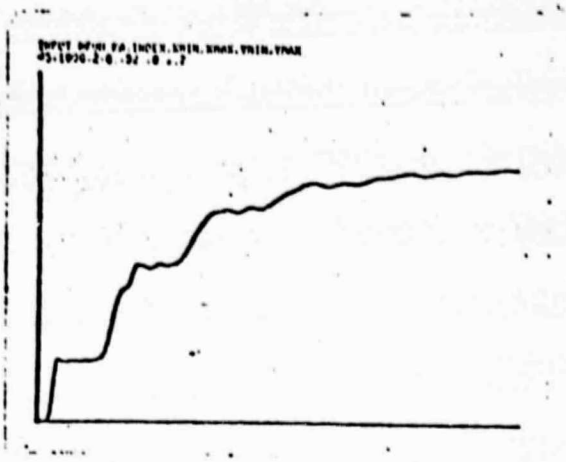

Fig. 10

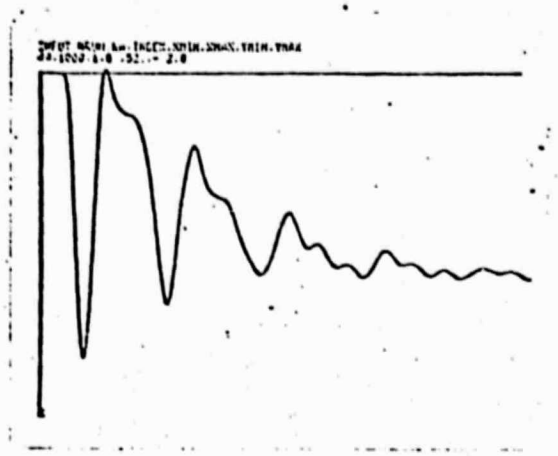

Fig. 11

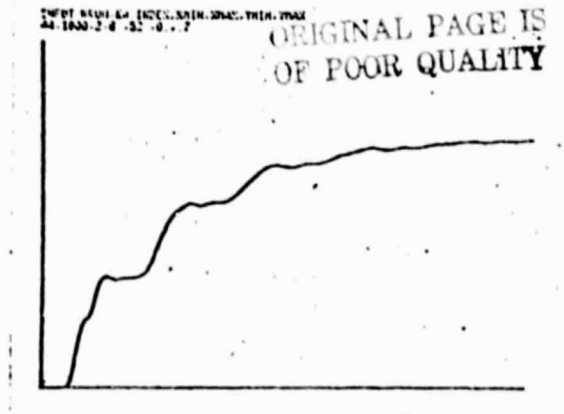

Fig. 12

sensitive parameter, indeed, and it is the proper indicator of local inaccuracies, when a steady state is apparently reached numerically. In this case, it is obvious that inaccuracies should be attributed to the vicinity of a singular point of the mapping and to the consequent worsening of the metric.

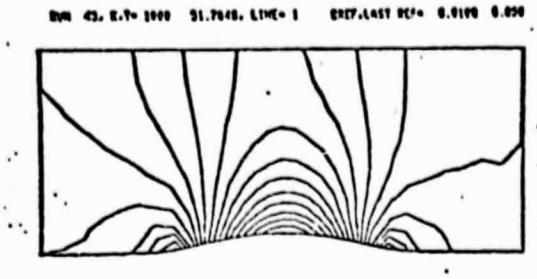

Fig. 13

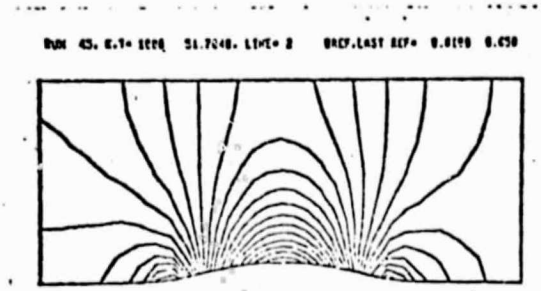

Fig. 14

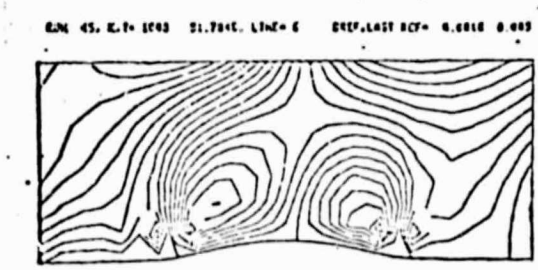

Fig. 15

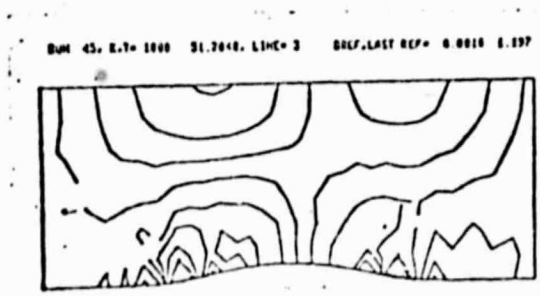

Fig. 16

Before going into the difficult problem of the corner singularity, it is proper to develop more familiarity with the wave propagation pattern for models 1 and 2, and their possible relationship with the existence of a bump. We have seen, so far, that waves tend to continue swaying back and forth, with very little damping, at low Mach numbers. To judge whether the geometry, and particularly the presence of a bump, has anything to do with the wave behavior, we examine two cases. One is an obvious choice, a straight channel with no bumps. It can be easily obtained from either the code using the Cartesian grid or the code using the mapping by setting the thickness of the bump equal to zero.

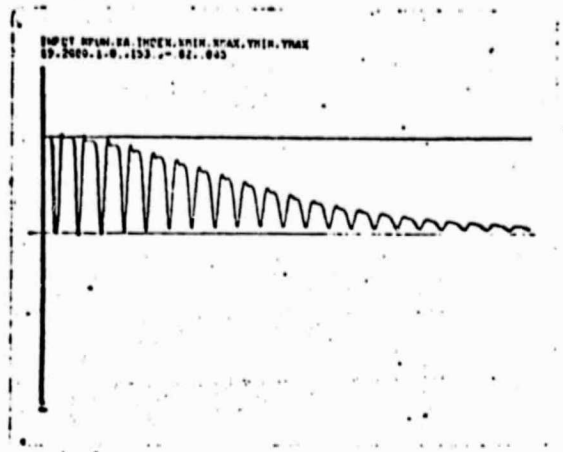

Fig. 17

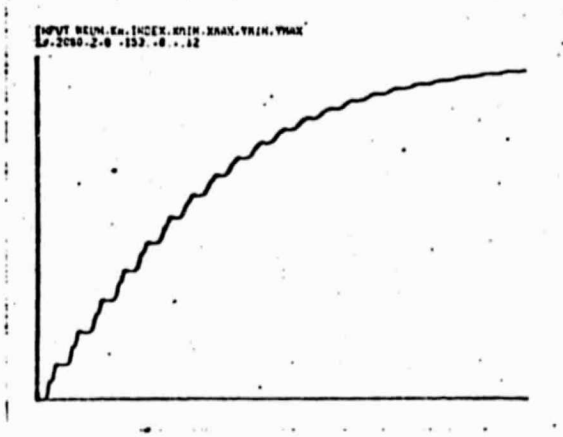

Fig. 18

Here are some results, for comparison with the previous cases. The first (Figs. 17 and 18) uses model 2, with a Mach number of 0.1. Compare Fig. 17 with Fig. 5 and Fig. 18 with Fig. 6. The second uses model 2 again, but with a Mach number equal to 0.5 (Figs. 19 and 20). Compare Fig. 19 with Fig. 11 and Fig. 20 with Fig. 12. Note that in this case the steady flow in the channel is uniform, with a pressure equal to the exit pressure; the transition from stagnation pressure (P=0) to the channel pressure takes place in the fictitious

transition which has been modeled at the inlet. In Figs. 21 (to be compared with Fig. 9) and 22 (to be compared with Fig. 10) the first model is used. Here the stagnation P is raised to a positive value and the exit P remains equal to zero; the latter is, thus, the asymptotic value of P in the whole

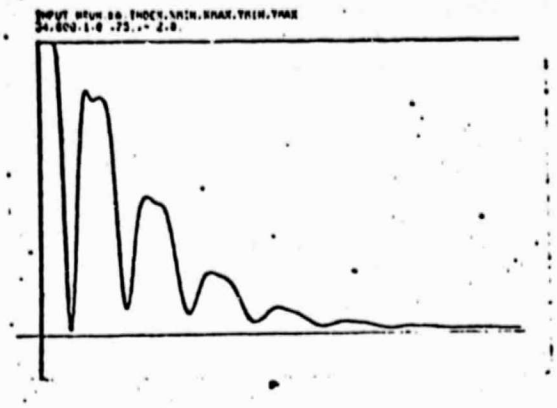

Fig. 19

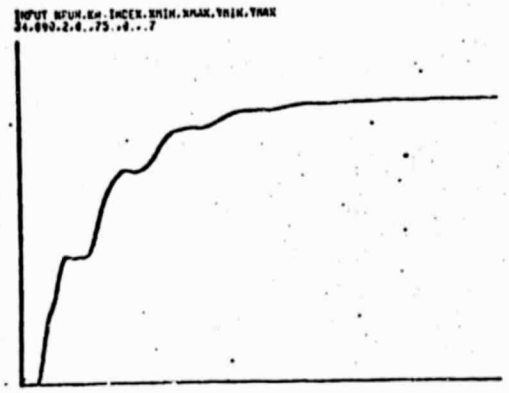

Fig. 20

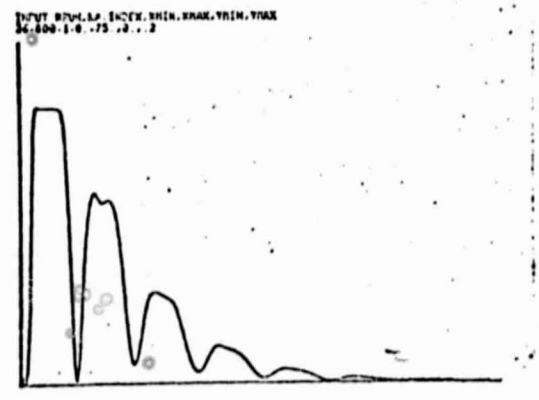

Fig. 21

channel.

All these patterns are similar to the ones with the bump; we can conclude that the oscillations are produced by the models of the boundaries

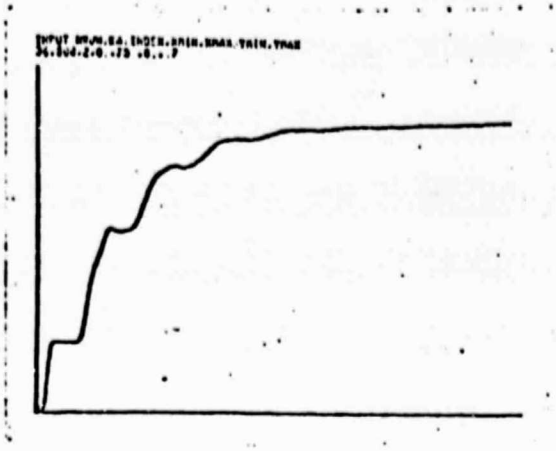

Fig. 22

and that they have a physical interpretation of their own, unrelated to the geometrical complications of the channel.

6. Two-dimensional calculations with model 3

We expect calculations made using the third model of Section 4 to converge to a steady state much faster than the previous ones, since the initial perturbation affects the entire flow field and whatever is not pertinent to the final state is promptly eliminated through the boundaries which, in this model, are not reflective. The expectations are confirmed by Figs. 23 and 24 (which should be compared with Figs. 4,5 and 6, respectively. Note also, in Figs. 25 and 26 (isobars and isomachs, respectively) how close the pattern is to the symmetric pattern of a steady state; compare these figures with Figs. 7 and 8. We omit presenting results for M=0.5; they are equally good and not dissimilar from the ones obtained using the second model, although a close inspection may reveal some advantage in using the third model (for example, the v=constant lines appear more symmetrical than in Fig. 15).

At this stage, we conclude that:

1) any one of the three models is acceptable as the description of a physical evolution,

2) any one of the three models is acceptable for the evaluation of a subsonic, steady state,

3) in any of the three models the computational region can be limited to a small portion of the channel, bracketing the bump,

4) the third model, however, provides faster convergence to a steady state, particularly for low Mach numbers.

Therefore, all further investigations will

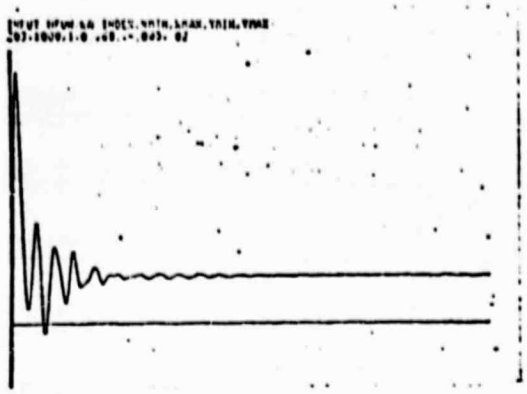

Fig. 23

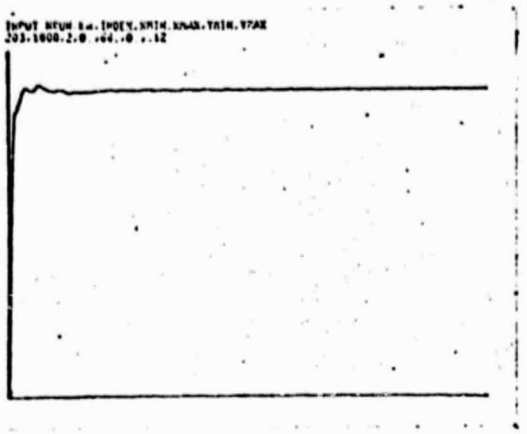

Fig. 24

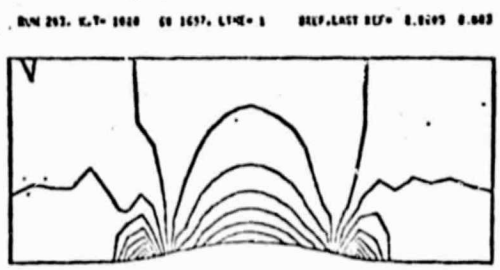

Fig. 25

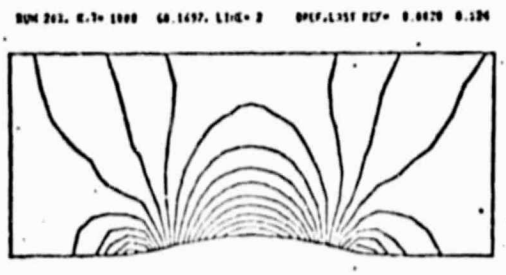

Fig. 26

be conducted using the third model.

7. The corner problem

We may turn now to the analysis of the difficulties arising when the lower wall has an actual corner. Probably, the first idea which may come to one's mind consists of performing successive calculations, with all parameters unchanged except b. Let us recall that all the preceding exercises have been performed with b=0.1, which corresponds to a rather smooth lower wall. What happens if b is reduced to 0.01, 0.001, and so on?

For b=0.01, and M=0.1, the P(t) and u(t) patterns do not show sizeable difference from the ones of Figs. 23 and 24 (b=0.1); the isobars and isomachs plots, however, start showing signs of degeneration near the corners, particularly the one on the left (Figs. 27 and 28). The region of high pressure tends to spread to the left, and the minimum Mach number is definitively misplaced. Minor changes in the rest of the plots can be ascribed to consequences of the poor accuracy near the corners. Although the calculation can be performed for much smaller values of b (even for b=0.0005) without catastrophies, such results can-

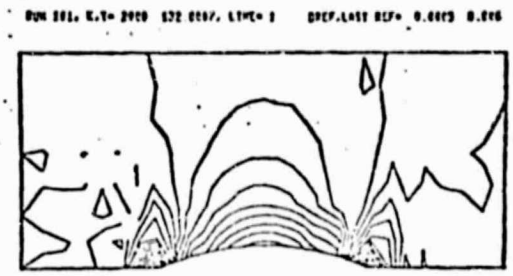

Fig. 27

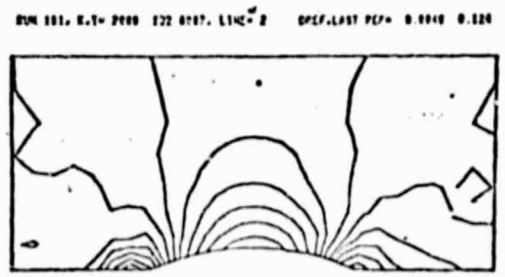

Fig. 28

not be considered realistic.

It is known [6] that the flow field at a corner is singular, so long as the corner angle is larger than 90°. Since the velocity vanishes at the corner, it will behave, in its immediate vicinity, as the velocity of an incompressible flow. Now, for the present case, the velocity of an in-

compressible flow along the lower wall is proportional to the G of (5). To learn more about u and its dependence on b, let us plot, in Fig. 29, a series of curves of G(x) for different values of b. In the same figure, arrows indicate the approximate positions of the nodal points for the computations

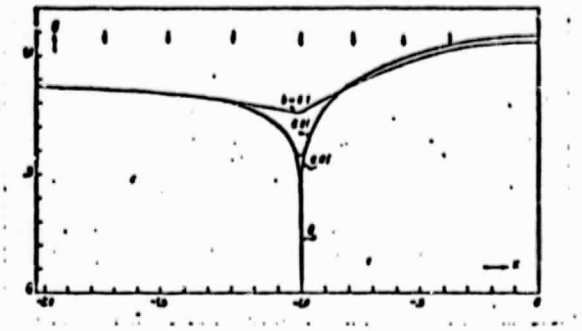

Fig. 29

shown in the preceding Sections.

The qualitative behavior of u is expected to follow the trends of Fig. 29, even in a compressible, unsteady flow. Similar considerations can be developed for P. At the corner itself, the only quantity to be computed is P, since u and v vanish identically. For all practical purposes, a reasonable estimate of P is obtained from the definition of the stagnation pressure, applied to values averaged on the 3 points surrounding the corner. Such an estimate tends to become more and more accurate as the flow approaches a steady state. The difficulty, thus, does not lie at the corner but at the neighborirg points. From Fig. 29 it is clear why a derivative such as u_x may be approximated by a 2-point difference if b=0.1 but the approximation is very poor if b=0.01 and it becomes disastrous if b=0. On the other hand, the values at the corner point cannot be just skipped because, if the derivatives at the neighboring points are approximated by one-sided differences only, all connection between the two sides of the corner is lost and, if the derivatives are approximated by differences between the two neighboring points, again the approximation is poor, as we can see from Fig. 29.

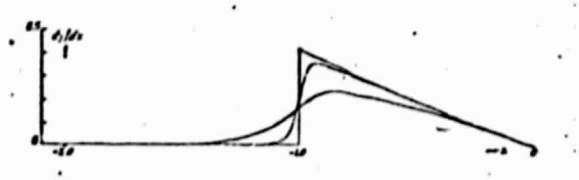

Fig. 30

If the Cartesian grid is used, the difficulty obviously persists. Plots of the slope of the lower wall are shown in Fig. 30 for various values of the parameter b. Again, for b=0 or close to it, the values at the corner can be determined without difficulty but the derivatives at the neighboring points are hard to approximate. Consequences similar to the ones observed in preceding Sections are visible in Figs. 31 and 32, where isomach lines are shown for the cases, b=0.1 and b=0.01, respectively.

Fortunately, the influence of the corner singularity is limited to a very small region surrounding the corner; in the grid used in our calculations, the departure of G from the very smooth curve, relative to b=0.1, occurs only inside one cell and differences between the curves relative to b=0.01 and b=0 appear only in a negligible portion of the cell. The motion in the neighborhood of the corner must be considered as the same which would take place in the presence of a fairing, such as the one defined by b=0.1, plus a sort of triangular region, comprising the corner, where the flow stagnates in a succession of quasi-steady states, even if the general motion is unsteady. Such a region should be considered only to evaluate the pressure at the corner, which should not be used, however, to compute derivatives at the neighboring points. It seems that analytic expressions for P and u within the corner cell, based on "reasonable" solutions for incompressible flow fail to provide the proper approximations to the derivatives, perhaps because their domain of validity is too small as compared with the size of the cell. A safer approach could consist of replacing the values of g and ϕ at the corners with their values at the corresponding point defined by b=0.1, say, in this way providing a localized fairing which should reflect the physical behavior, maintaining a geometry which would not conflict with continuity requirements and producing values for pressure and velocity components which could be used directly for the approximation of derivatives. More on this subject, including a study of different corner angles, down to the limiting (and very special) case of a

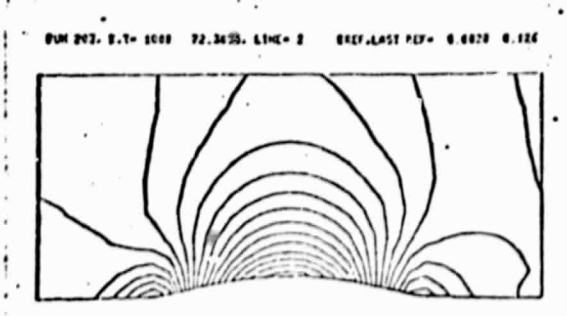

Fig. 31

90° corner, will appear in a forthcoming paper.

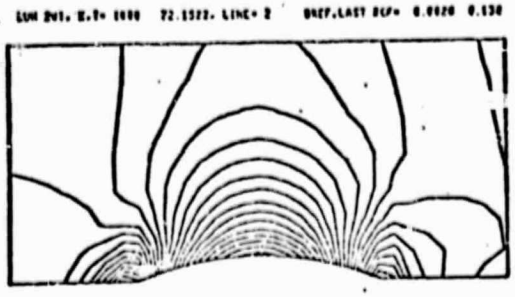

Fig. 32

Acknowledgment.
Part of this work was sponsored by the NASA Langley Research Center under Grant No. NSG 1248 and performed during the Author's visit at ICASE in August 1980.

References.

1. Perry, J., "A comparison of solutions to some blunt body problems," AIAA J. 4, 1425-1426 (1966)
2. Moretti, G. and Abbett, M., "A time-dependent computational method for blunt body flows," AIAA J. 4, 2136-2141 (1966)
3. Abbett, M.J., "Boundary condition calculation procedures for inviscid supersonic flow fields," Proc. AIAA Comp. Fl. Dyn. Conf., Palm Springs, 153, 1973
4. deNeef, T., "Treatment of boundaries in usteady inviscid flow computations," Delft Univ. of Techn., Dept. of Aerosp. Eng. Rep. LR-262 (1978)
5. Moretti, G. and Pandolfi, M., "On the calculation of subsonic flows in ducts,", POLY M/AE Rep. No. 80-18 (1980)
6. Pandolfi, M. and Zannetti, L., "A physical approach to solve numerically complicated hyperbolic flow problems," VII Int. Conf. on Num. Meth. in Fluid Dyn. (1980)
7. Van Dyke, M.D., Perturbat on Methods in Fluid Mechanics, Parabolic Press (1975)